Theoretical study on Curcumin: A comparison of calculated spectroscopic properties with NMR, UV–vis and IR experimental data

ARTICLE *in* JOURNAL OF MOLECULAR STRUCTURE · DECEMBER 2008

Impact Factor: 1.6 · DOI: 10.1016/j.molstruc.2008.05.024

Journal of Molecular Structure 892 (2008) 168–176

Contents lists available at ScienceDirect

Journal of Molecular Structure

journal homepage: www.elsevier.com/locate/molstruc

Theoretical study on Curcumin: A comparison of calculated spectroscopic properties with NMR, UV–vis and IR experimental data

Rois Benassi *, Erika Ferrari, Sandra Lazzari, Ferdinando Spagnolo, Monica Saladini

Department of Chemistry, University of Modena and Reggio Emilia, via Campi 183, 41100 Modena, Italy

ARTICLE INFO

Article history:
Received 19 March 2008
Received in revised form 7 May 2008
Accepted 11 May 2008
Available online 21 May 2008

Keywords:
Curcumin
DFT calculations
NMR
Spectroscopic properties

ABSTRACT

The main target of this study is a high-level computational analysis of Curcumin, employing DFT approach with two different sets of basis functions (B3LYP/6-31G* and B3LYP/6-311G**). Accurate quantum mechanical studies, both *in vacuum* and in methanol medium, are carried out with the aim to analyze the conformational equilibria, to find the most stable equilibrium structure and to define the nature of the molecular orbitals, fundamental to explain Curcumin binding characteristic. Our theoretical calculations, performed at B3LYP/6-31G* and B3LYP/6-311G** levels both *in vacuum* and in methanol medium, confirm that the keto-enolic forms are more stable than the di-keto one, whose extremely low population suggests that this structure should not influence Curcumin properties. Keto-enolic form C results the most stable, independently on calculation level and solvent (methanol) effect. HOMO and LUMO molecular orbitals are calculated for all the structures with the two sets of basis with very similar results. MEPs show that the negative charge is localized on the oxygen atoms, which, in the keto-enolic forms, point in the same direction enabling metal coordination.

NMR, UV–vis and FT-IR experimental data are employed in the comparison with electronic and conformational properties of Curcumin resulting from theoretical calculations. The two different calculation levels (B3LYP/6-31G* and B3LYP/6-311G**) give very similar results.

Good linear correlations between the experimental ^{1}H and ^{13}C NMR chemical shifts (δ_{exp}), in methanol-d_4 (MeOD) and DMSO-d_6 (DMSO), and calculated magnetic isotropic shielding tensors (σ_{calc}) are found ($\delta_{exp} = a \cdot \sigma_{calc} + b$). A good prediction of UV–vis experimental maximum absorption (λ_{max}) on the basis of conformer populations is obtained. A linear relation with a good correlation coefficient is observed plotting the FT-IR experimental wavenumbers vs. the calculated ones, allowing to predict FT-IR spectra.

1. Introduction

Curcumin (Fig. 1) the active yellow pigment obtained from the dried rhizomes of *Curcuma longa* L., is a popular coloring spice and ingredient of many cosmetics and pharmaceuticals [1–3]. Curcumin has been generally associated with a large number of biological and cellular activities, including antioxidant, anti-inflammatory, anticarcinogenic, and hypocholesterolemic properties [2–4]. In addition it is reported that Curcumin is able to induce apoptosis in human cancer cells of different tissue origin, including B and T cells, colon, epidermis, prostate, breast and head [5–7]. A photolysis study by Jovanovic et al. attributes the antioxidant mechanism of Curcumin to intermolecular H-atom transfer in the keto-enolic group [8]. A recent theoretical study by Balasubramanian suggests that the keto-enolic form of Curcumin may be responsible for the inhibition of β-amyloid aggregation [9]. Curcumin has also shown to be able to act as chelating agent towards Ga^{3+} and Fe^{3+} [10], and it is therefore under investigation as potential Ga^{3+}/Fe^{3+} pharmaceutical carrier in anti-cancer therapy and in the treatment of iron-deficiency pathologies. However, the nature of many biological properties of Curcumin remains unclear; therefore, it is important to investigate the structure and reactivity of this prolific medicinal agent.

The main target of this study is a high-level computational analysis of Curcumin employing DFT approach with two different sets of basis functions (B3LYP/6-31G* and B3LYP/6-311G**). Accurate quantum mechanical studies on Curcumin, both *in vacuum* and in methanol medium, are here carried out with the aim to analyze the conformational equilibria, to find the most stable equilibrium structure and to define the nature of the molecular orbitals, particularly the highest occupied and lowest unoccupied ones that are important to explain binding characteristic. NMR, UV–vis and FT-IR experimental data are employed in the comparison with electronic and conformational properties of Curcumin resulting from theoretical calculations.

* Corresponding author. Tel.: +39 0592055046; fax: +39 059373543.
E-mail address: rois.benassi@unimore.it (R. Benassi).

0022-2860/$ - see front matter © 2008 Elsevier B.V. All rights reserved.
doi:10.1016/j.molstruc.2008.05.024

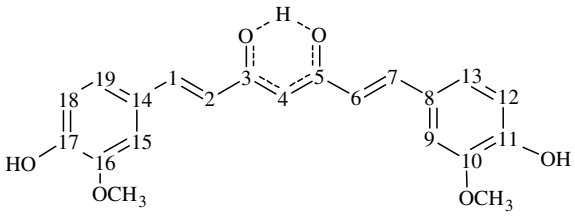

Fig. 1. Structure of Curcumin with numbering atoms.

2. Experimental

2.1. Computational details

All the calculations are performed with Gaussian 03 [11] package of programs. The geometry of all involved structures is fully optimised with the DFT methodology, using the three-parameter hybrid-functional of Becke [12–13] combined with the B3LYP/6-31G* and B3LYP/6-311G** basis sets. Thermodynamic data are obtained from vibrational analysis, employing general procedures. Then, using these structures as starting points, the absorption wavelengths and oscillator strengths are calculated by means of time-dependent density functional theory (TD-DFT) [14], using the same basis sets. The molecular electrostatic potential maps (MEP) [15] of the optimized geometry structures of Curcumin and its derivatives are calculated at the same level of theory and plotted using Gaussview [16]. MEPs are reported onto 0.02 *e*/Bohr isosurface of electrodensity, representations of HOMO and LUMO orbital density refer to an isovalue of 0.0004. The solvent (MeOH) effects are evaluated by employing the self-consistent reaction field (SCRF) method with polarized *continuum* model (PCM) [17–19].

The magnetic isotropic shielding tensors (σ) for ^{1}H and ^{13}C NMR are calculated using the standard GIAO (Gauge-Independent Atomic Orbital) [20] at B3LYP/6-31G* and B3LYP/6-311G** approach with the Gaussian 03 program package.

2.2. Spectroscopy

NMR spectra are recorded at 300 K on a Bruker Avance AMX-400 spectrometer with a Broad Band 5-mm probe (inverse detection). Nominal frequencies are 100.13 MHz for ^{13}C and 400.13 MHz for ^{1}H. The typical acquisition parameters for ^{1}H are as follows: 20 ppm spectral bandwidth (SW), 6.1 μs pulse width (90° pulse hard pulse on ^{1}H), 0.5- to 1-s pulse delay, 216–512 number of scans. For 2D H,H-Homonuclear Correlated Spectroscopy (COSY [21]) typical parameters were used. For 2D H,X-Hetero Correlated Spectroscopy (HMBC [22] and HMQC [23]) opportune parameters were used (50–90° pulses; 32 k data points; 1 s relaxation delay; 8–64 k transients; $^{1}J_{H-C}$ 125–145 Hz; $^{3}J_{H-C}$ 5–15 Hz). Methanol-d_4 (MeOD) and DMSO-d_6 (DMSO) are used as NMR solvent.

UV–vis measurements are performed using Jasco V-570 spectrophotometer at 25.0 ± 0.1 °C in the 200–600 nm spectral range employing a 1 cm quartz cell, a 2.5×10^{-5} M methanolic Curcumin solution is used for acquisition.

The infrared spectrum of Curcumin is obtained by means of a Bruker FTIR VERTEX 70, with a MCT Mid-Band detector in the 4000–600 cm^{-1} spectral range using an ATR Golden-Gate (Heated-Diamond top-plate).

3. Results and discussion

3.1. Theoretical calculation

From X-ray crystallography [24–25] the existence, in the solid state, of at least two Curcumin conformers (Fig. 2A and B types) is known. Previous theoretical calculations [10,26–29] report three structures (Fig. 2A, C and D), which were considered without a direct comparison. In the present work we investigate all possible Curcumin conformers in order to establish a reliable starting point to further theoretically explore the complexing ability of Curcumin and its derivatives towards metal ions.

Curcumin possesses two isomers: di-ketonic and keto-enolic ones which may assume different conformations. The final opti-

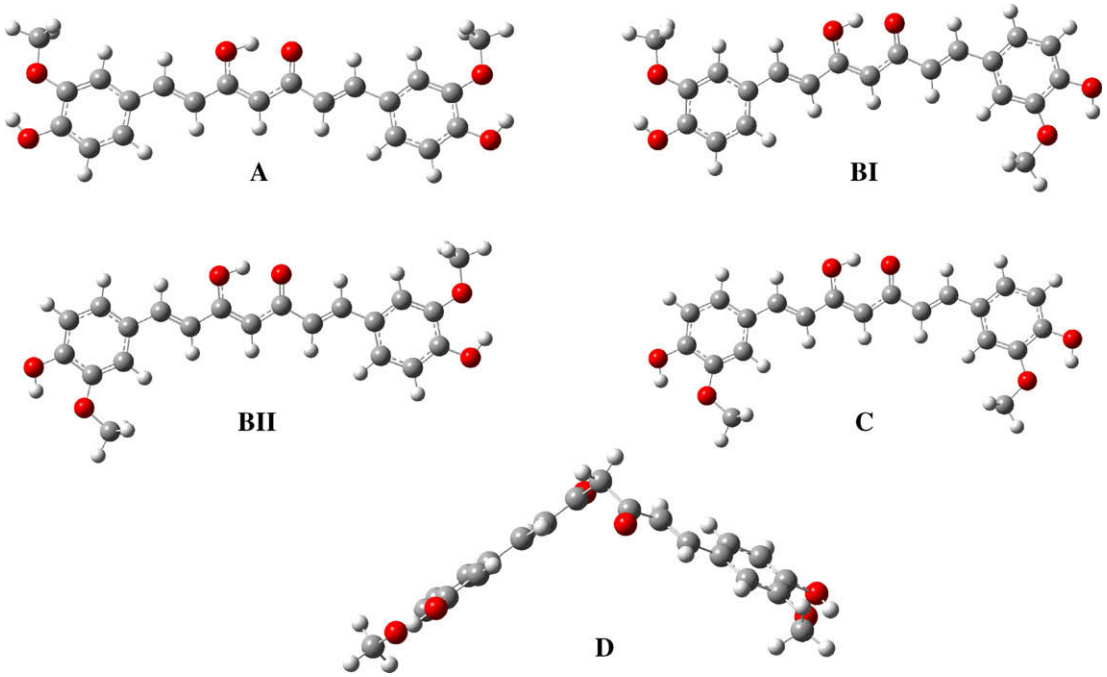

Fig. 2. The final optimized structures of Curcumin conformers at B3LYP/6-311G** level.

mized structures for B3LYP/6-311G** are shown in Fig. 2. Calculated values for keto-enolic and di-ketonic structures are reported in Table 1.

ΔE, Δ(E + ZPE), ΔG and ΔH values are calculated with two different atomic sets of basis (B3LYP/6-31G* and B3LYP/6-311G**) and the results are very similar, generating an equivalent order of stability among the different species. The same equivalence between the two basis is maintained in molecular geometry calculations; Curcumin keto-enolic structures (A, BI, BII and C), independently on the used set of basis, are completely planar: bond length deviations are within ±0.003 Å, while bond angle and dihedral angle deviations are within ±0.09° and ±0.01°, respectively.

Our theoretical calculation confirms that the keto-enolic forms are more stable than the di-keto one (D) as previously observed [9,26–29]. The extremely low value of D population, calculated *in vacuum* as well as in solvent medium, suggests that this form should not influence Curcumin properties.

The most stable keto-enolic species depends on the energy terms taken into account: if ΔE, ΔE + ZPE) and ΔH are considered BII outcomes the most stable, otherwise, if ΔG term is considered, C results the most stable. The energy gap between these two species is anyway very small.

The crystal structure reports the enolic hydrogen equally shared by the two oxygen atoms of the keto-enolic moiety, while calculations show two distinct energetically equivalent keto-enolic forms for both A and C, since the two possible keto-enolic resonance structures are equivalent. The tautomeric equilibrium between the two resonance forms occurs through a transition state with a ΔG^* of 0.44 kcal/mol for B3LYP/6-31G* and 0.17 kcal/mol for B3LYP/6-311G**. The extremely low energetic requisite gives an equilibrium in fast exchange in solution, and the active state corresponds to the crystal structure with the hydrogen atom equidistant from the two oxygen atoms. B structure is swapped in the two conformers BI and BII, not symmetrically equivalent, but with a very low energetic gap (Δ (ΔG) 0.01 kcal/mol for B3LYP/6-31G* and 0.0 kcal/mol for B3LYP/6-311G**). All the structures show two intramolecular hydrogen bonds involving phenolic hydrogen and methoxylic oxygen (H···O 2.07 Å). The difference in stability between the four keto-enolic conformers (A, BI, BII and C) is very low as regarding Δ(*E* + ZPE) and slightly higher concerning ΔG. We assume that all the keto-enolic structures can coexist in standard conditions (298.75 K, 1 atm) as a consequence of the possible free rotation around the single bond connecting the aromatic ring with the dienic structure; in fact the calculated rotational energy barrier is rather low (ΔG^* 7.70 and 8.01 kcal/mol, respectively, for B3LYP/6-31G* and B3LYP/6-311G** for the rotation of a phenyl ring in conformer C). These results justify the presence of the two different X-ray structures reported in literature [24–25].

MeOH medium is chosen for calculations as it is the solvent used to perform solution study of Curcumin, in particular to collect NMR and UV–vis experimental data.

Solvent effect is irrelevant in relation to stability and conformation equilibria of Curcumin, as it is highlighted by the comparison of population data (Table 1).

HOMO and LUMO molecular orbitals are calculated for all the structures with the two set of basis, giving rise to very similar results. A, BI, BII and C show a great similarity (Fig. 3); in these structures HOMO and LUMO are delocalized on the entire molecule, being the electronic density distributed both in the dienic part of the molecule and in benzenic one. For the di-ketonic structure (D) the last two occupied molecular orbitals (HOMO and HOMO-1) are almost degener (−0.209 and 0.204 eV and −0.218 and 0.213 eV, respectively, for B3LYP/6-31G* and B3LYP/6-311G**), each is delocalized on half molecule giving rise to two separated fragments. This accounts for the higher stability of A, BI, BII and C conformers with respect to D, suggesting their ability to chelate metal ions as previously observed [10].

MEPs [15] are calculated for all the optimized structures, C and D forms are shown in Fig. 4. In all the structures the negative charge is localized on the oxygen atoms, which, in the keto-enolic forms, point in the same direction enabling metal coordination. Charge density values of oxygen atoms, reported in Table 2, hint the same chelating capability for A, BI, BII and C.

In the di-ketonic form the coordination is allowed only upon rotation of the di-keto structure (ΔG^* value of 4.01 and 1.81 kcal/mol, respectively, for B3LYP/6-31G* and B3LYP/6-311G**) followed by the tautomeric equilibrium, that needs a very high energy barrier, as previously reported for acetylacetone [30].

3.2. NMR spectroscopy

Fig. 5 (bottom) reports ^{1}H NMR spectrum of Curcumin in DMSO; ^{1}H and ^{13}C chemical shift assignments (Tables 3 and 4) are supported by 2D COSY, HSQC and HMBC experiments. The fit between experimental chemical shifts (δ) of Curcumin in DMSO and MeOD for both ^{1}H and ^{13}C (Fig. 5A and B, respectively) illustrates very small variation due to experimental conditions, suggesting irrelevant solvent effects.

Experimental data evidence only one set of signals corresponding to an averaged chemical species of all keto-enolic possible structures of Curcumin (A, BI, BII and C) in fast equilibrium in

Table 1
The total electronic energies (*E*), zero point vibrational energies (*E* + ZPE), thermodynamics quantities (*G*, *H* and *S*), relative differences *in vacuum*, free energy of solvation (ΔG_{solv}), free energy differences in solution (ΔG_{MeOH}) and relative conformational population *in vacuum* (N_v) and in solution (N_{MeOH})

	E[a]	E + ZPE[a]	G[a]	H[a]	S[b]	ΔE[c]	Δ (E + ZPE)[c]	ΔG[c]	ΔH[c]	ΔG_{solv}[c]	ΔG_{MeOH}[c]	N_v	N_{MeOH}
*B3LYP/6-31G**													
A	−1263.573127	−1263.201114	−1263.260810	−1263.174611	181.421	0.149	0.169	0.395	0.187	−15.980	0.275	0.224	0.261
BI	−1263.573300	−1263.201363	−1263.260548	−1263.174888	180.289	0.033	0.013	0.559	0.013	−15.880	0.539	0.169	0.167
BII	−1263.573348	−1263.201384	−1263.260562	−1263.174909	180.272	0.000	0.000	0.550	0.000	−15.840	0.571	0.172	0.158
C	−1263.573277	−1263.201358	−1263.261439	−1263.174869	182.202	0.048	0.016	0.000	0.025	−15.860	0.000	0.435	0.414
D	−1263.566078	−1263.194527	−1263.255945	−1263.167534	186.078	4.889	4.303	3.447	4.628	−16.580	2.728	0.001	0.004
*B3LYP/6-311G***													
A	−1263.917090	−1263.547413	−1263.606960	−1263.520864	181.204	0.172	0.190	0.270	0.205	−17.090	0.150	0.234	0.269
BI	−1263.917292	−1263.547693	−1263.606806	−1263.521174	180.226	0.036	0.014	0.367	0.010	−17.010	0.327	0.199	0.200
BII	−1263.917346	−1263.547715	−1263.606806	−1263.521190	180.193	0.000	0.000	0.367	0.000	−16.960	0.377	0.199	0.184
C	−1263.917300	−1263.547707	−1263.607391	−1263.521188	181.430	0.030	0.000	0.000	0.001	−16.970	0.000	0.369	0.347
D	−1263.905684	−1263.536591	−1263.597850	−1263.509566	185.809	7.843	6.980	5.987	7.294	−17.900	5.057	1.5E−5	6.6E−5

[a] a.u.
[b] cal mol^{-1} K^{-1}.
[c] kcal mol^{-1}.

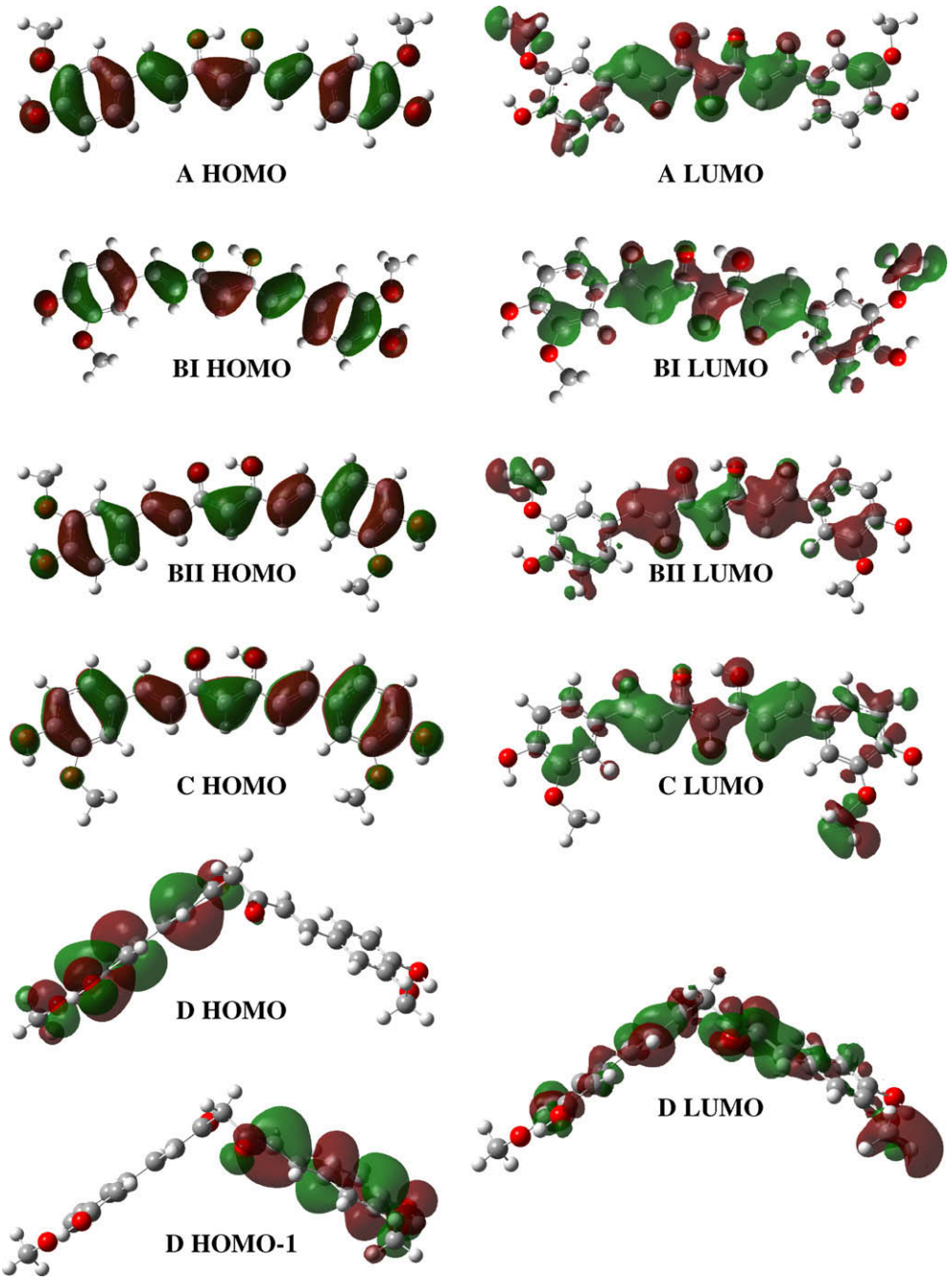

Fig. 3. Representations of HOMO and LUMO orbital density of Curcumin conformers at B3LYP/6-311G** level.

NMR time scale; resonances show a completely symmetric species (C_{2v}): (a) the enolic proton is equally shared between the two oxygen atoms of keto-enolic structure and strongly deshielded due to its involvement in a hydrogen bond; (b) ketonic carbon and enolic carbon are undistinguishable and equivalent, showing a ^{13}C δ value of 183.6 ppm; (c) the two aromatic rings and the double bonds are completely equivalent.

Tables 3 and 4 show the GIAO (Gauge-Independent-Atomic-Orbitals) isotropic magnetic shielding tensors (σ_{calc}) for all refined keto-enolic structures (A, BI, BII and C) for both calculation levels.

$\bar{\sigma}_{calc}$ are obtained on the basis of the relative species populations:

$$\bar{\sigma}_{calc} = \sigma_{calc}(A) \cdot n_A + \sigma_{calc}(BI) \cdot n_{BI} + \sigma_{calc}(BII) \cdot n_{BII} + \sigma_{calc}(C) \cdot n_C$$

n_A, n_{BI}, n_{BII} and n_C population are calculated according to the ΔG values excluding the di-keto form; $\sigma_{calc}(A)$ and $\sigma_{calc}(C)$ are the averaged values of isotropic shielding tensors of the two resonance forms of A and C, respectively.

Plotting the experimental ^{13}C and ^{1}H chemical shifts (δ_{exp}) in MeOD and DMSO vs. the σ_{calc} for all species (or $\bar{\sigma}_{calc}$), a linear regression is obtained: $\delta_{exp} = a \cdot \sigma_{calc} + b$ (a, b and R^2 parameters are give in Tables 3 and 4). This relationship is used to predict the chemical shifts (δ_{pred}). As already observed [31], the correlation between experimental chemical shifts and calculated isotropic screening constants for ^{13}C is better than for ^{1}H (Fig. 6), in fact an homogeneous behaviour is observed for ^{13}C independently on the calculated species with a correlation coefficient R^2 ranging from 0.9691 to 0.9917. Fig. 6A shows ^{13}C δ_{exp} vs. $\bar{\sigma}_{calc}$ while

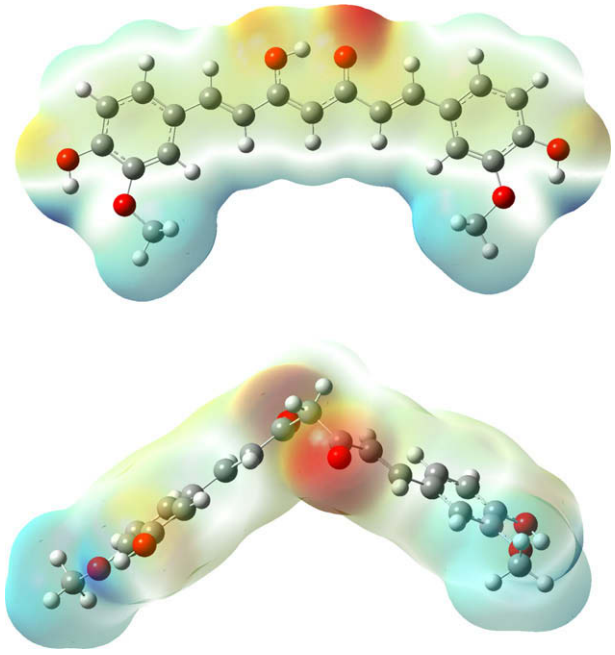

Fig. 4. Molecular electrostatic maps of Curcumin C (up) and D (bottom) at B3LYP/6-311G** level.

Table 2
CHELPG[a] charges on the keto-enolic two oxygen atoms of Curcumin isomers

	B3LYP/6-31G*		B3LYP/6-311G**	
	C=O	C–OH	C=O	C–OH
A	−0.595	−0.579	−0.621	−0.600
BI	−0.596	−0.583	−0.618	−0.598
BII	−0.598	−0.575	−0.624	−0.592
C	−0.601	−0.584	−0.627	−0.605

[a] As implemented in Gaussian 03 [11] package.

Fig. 6B reports the ^{1}H δ_{exp} vs. σ_{calc}(C), since C is the species that better predicts the experimental behaviour for proton (R^2 = 0.9273).

Solvent effects seems to be irrelevant in order to predict experimental chemical shifts, in fact the GIAO (Gauge-Independent-Atomic-Orbitals) isotropic magnetic shielding tensors (σ_{calc}) calculated *in vacuum* and in MeOH medium give rise to very similar results (supplementary material).

Almost identical outputs are obtained using the two calculation levels (B3LYP/6-31G* and B3LYP/6-311G**).

3.3. UV–vis spectroscopy

Table 5 reports theoretical and experimental UV–vis data; it is evident that the use of the two different sets of basis leads to comparable results, both as it concerns absorption wavelength (λ) and oscillator strength (f) values. The four conformers A, BI, BII and C show a calculated maximum absorption very similar; the value of λ_{max} averaged on the basis of conformer populations is 416 nm and 419 nm, respectively, for B3LYP/6-31G* and B3LYP/6-311G**, both very close to the experimental value of Curcumin (417 nm in benzene [32], 419 nm in chloroform [33] and 420 nm in methanol). The rather high oscillator strength is consistent with the experimentally observed strong absorption spectrum of the keto-enolic form [29].

3.4. Infra red spectroscopy

Fig. 7 reports the solid state measured FT-IR spectrum of Curcumin compared with the calculated one obtained taking into account the relative weight of each keto-enolic isomer. Usually the calculated harmonic vibrational wavenumbers are higher than the experimental ones, because of the anharmonicity, of the incomplete treatment of electron correlation and of the use of finite one-particle basis set [34]. A linear relation with a good correlation coefficient is obtained plotting the experimental wavenumbers vs. the calculated ones ($\bar{\nu}_{calc}$) (Table 6 and Fig. 8),

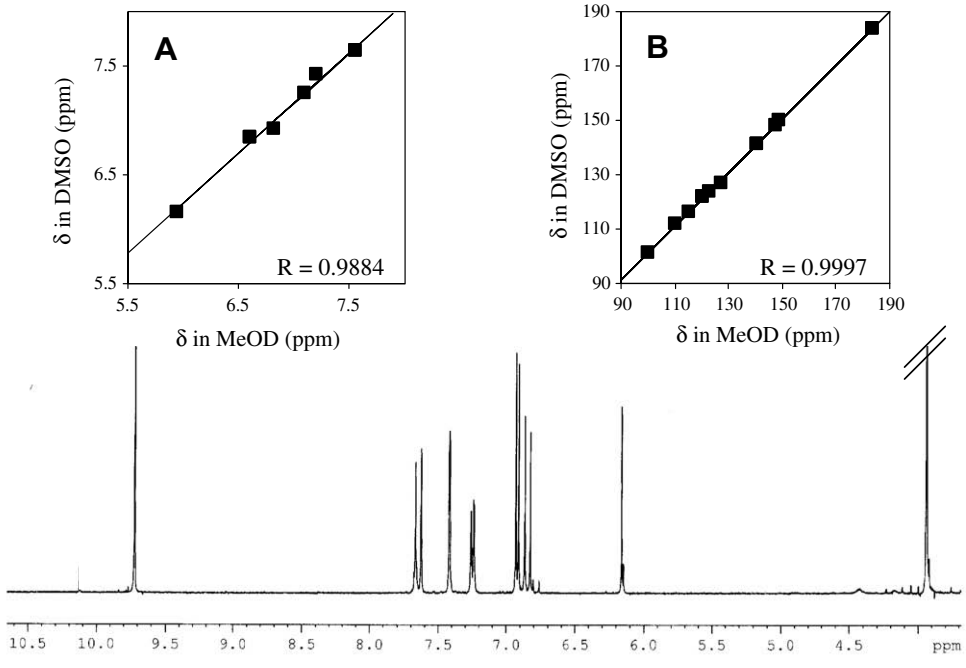

Fig. 5. ^{1}H NMR spectrum of Curcumin in DMSO (bottom). Plots of DMSO vs. MeOD Curcumin experimental chemical shifts (δ) for ^{1}H (A) and ^{13}C (B).

Table 3
Experimental (MeOD and DMSO) ^{13}C chemical shifts (δ_{exp}, ppm), predicted ^{13}C chemical shifts ($\delta_{pred} = a \cdot \bar{\sigma}_{calc} + b$, ppm) and calculated GIAO magnetic isotropic shielding tensors (σ_{calc} and $\bar{\sigma}_{calc}$) for Curcumin

^{13}C	MeOD			DMSO			σ_{calc}*				$\bar{\sigma}_{calc}$*	σ_{calc}**				$\bar{\sigma}_{calc}$**
	δ_{exp}	δ_{pred}*	δ_{pred}**	δ_{exp}	δ_{pred}*	δ_{pred}**	A	BI	BII	C		A	BI	BII	C	
1	140.4	142.2	142.0	141.1	142.7	142.6	55.37	56.55	54.24	54.98	55.17	36.26	39.14	36.38	37.05	37.15
2	120.6	120.0	120.1	121.6	121.0	121.0	74.73	76.44	73.09	75.66	75.22	58.82	60.34	57.37	60.08	59.31
3	183.7	182.8	181.0	183.6	182.7	180.9	18.35	25.73	11.19	18.42	18.40	−2.25	4.17	−8.49	−2.23	−2.20
4	100.2	104.6	101.6	101.2	105.8	102.9	88.89	89.01	89.07	89.30	89.14	77.69	77.83	77.85	78.21	77.95
5	183.7	182.8	181.0	183.6	182.7	180.9	18.35	11.11	25.53	18.42	18.39	−2.25	−8.63	4.03	−2.23	−2.26
6	120.6	119.8	119.6	121.6	120.8	120.6	74.73	73.88	77.26	75.66	75.39	58.82	58.50	61.47	60.08	59.75
7	140.4	142.3	141.9	141.1	142.8	142.5	55.37	53.81	56.07	54.98	55.08	37.68	35.76	38.48	37.05	37.23
8	127.3	126.9	128.2	126.8	127.7	129.0	68.94	69.01	68.96	68.97	68.96	51.07	51.11	51.09	51.14	51.11
9	110.1	106.3	104.8	111.9	107.5	106.0	80.91	89.96	90.35	90.13	87.64	67.21	76.93	77.32	76.96	74.75
10	147.8	146.2	147.6	148.4	146.8	148.0	51.82	51.40	51.23	51.35	51.47	32.00	31.50	31.32	31.40	31.55
11	149.0	150.0	151.6	149.8	150.5	152.0	48.46	47.79	47.99	47.86	48.03	27.93	27.20	27.42	27.36	27.48
12	115.0	113.3	114.1	116.2	114.4	115.1	80.81	81.46	81.41	81.49	81.30	64.72	65.62	65.56	65.60	65.40
13	122.6	126.6	126.7	123.5	127.5	127.6	76.08	66.32	67.08	66.66	69.22	60.12	49.97	50.82	50.22	52.61
14	127.3	126.9	128.2	126.8	127.8	129.0	68.94	68.83	68.87	68.97	68.94	51.07	51.02	51.03	51.14	51.08
15	110.1	108.3	108.7	111.9	109.5	109.8	80.91	81.39	80.70	90.13	85.77	67.21	67.68	66.92	76.96	70.85
16	147.8	146.1	147.3	148.4	146.6	147.8	51.82	51.80	51.84	51.35	51.57	32.00	32.01	32.05	31.40	31.79
17	149.0	149.9	151.4	149.8	150.4	151.8	48.46	48.43	48.26	47.86	48.12	27.93	27.87	27.69	27.36	27.66
18	115.0	113.4	114.4	116.2	114.5	115.5	80.81	80.79	80.94	81.49	81.18	64.72	64.58	64.75	65.60	65.03
19	122.6	124.5	122.9	123.5	125.4	123.8	76.08	76.33	75.93	66.66	71.16	60.12	60.38	59.98	50.22	56.50
MeOD																
a							−1.1306	−1.0852	−1.0847	−1.0740	−1.1050	−1.0134	−0.9762	−0.9767	−0.9592	−0.9897
b							204.725	201.867	201.835	201.177	203.124	179.774	178.177	178.203	177.418	178.784
R^2							0.9910	0.9691	0.9697	0.9772	0.9917	0.9934	0.9749	0.9754	0.9759	0.9910
DMSO																
a							−1.1126	−1.0670	−1.0666	−1.0553	−1.0864	−0.9969	−0.9596	−0.9601	−0.9423	−0.9728
b							204.312	201.447	201.417	200.723	202.672	179.744	178.140	178.167	177.367	178.734
R^2							0.9915	0.9680	0.9687	0.9748	0.9903	0.9932	0.9732	0.9738	0.9730	0.9892

The numbering of atoms refers to Fig. 1.
* Calculation performed at B3LYP/6-31G* level.
** Calculation performed at B3LYP/6-311G** level.

Table 4
Experimental (MeOD and DMSO) ^{1}H chemical shifts (δ_{exp}, ppm), predicted ^{1}H chemical shifts ($\delta_{pred} = a\bar{\sigma}_{calc} + b$, ppm) and calculated GIAO magnetic isotropic shielding tensors (σ_{calc} and $\bar{\sigma}_{calc}$) for Curcumin

^{1}H	MeOD			DMSO			σ_{calc}*				$\bar{\sigma}_{calc}$*	σ_{calc}**				$\bar{\sigma}_{calc}$**
	δ_{exp}	δ_{pred}*	δ_{pred}**	δ_{exp}	δ_{pred}*	δ_{pred}**	A	BI	BII	C		A	BI	BII	C	
1	7.56	7.42	7.48	7.64	7.54	7.59	24.95	25.04	24.83	24.87	24.91	24.25	24.35	24.14	24.19	24.23
2	6.61	6.64	6.64	6.85	6.83	6.84	26.10	26.25	26.00	26.27	26.18	25.48	25.63	25.38	25.65	25.55
4	5.95	5.94	5.98	6.15	6.20	6.23	27.28	27.32	27.32	27.36	27.33	26.57	26.60	26.60	26.63	26.61
6	6.61	6.61	6.61	6.85	6.81	6.81	26.10	26.12	26.38	26.27	26.23	25.48	25.49	25.75	25.65	25.60
7	7.56	7.42	7.49	7.64	7.54	7.60	24.95	24.80	25.01	24.87	24.90	24.25	24.10	24.31	24.19	24.21
9	7.20	7.02	7.00	7.42	7.18	7.16	25.95	25.40	25.47	25.45	25.56	25.35	24.83	24.90	24.89	24.99
12	6.82	7.04	7.00	6.92	7.20	7.16	25.49	25.54	25.55	25.52	25.52	24.93	25.00	25.01	24.99	24.98
13	7.09	7.17	7.15	7.25	7.32	7.30	24.89	25.38	25.47	25.43	25.31	24.35	24.83	24.92	24.86	24.75
15	7.20	6.91	6.87	7.42	7.08	7.04	25.95	26.00	25.90	25.45	25.73	25.35	25.42	25.34	24.89	25.20
18	6.82	7.05	7.02	6.92	7.21	7.17	25.49	25.50	25.51	25.52	25.50	24.93	24.94	24.95	24.99	24.96
19	7.09	7.28	7.28	7.25	7.42	7.41	24.89	24.93	24.86	25.43	25.13	24.35	24.41	24.34	24.86	24.55
MeOD																
a							−0.5161	−0.5711	−0.5685	−0.6258	−0.6115	−0.5432	−0.595	−0.5927	−0.6548	−0.6334
b							20.189	21.611	21.546	23.023	22.648	20.549	21.862	21.807	23.372	22.827
R^2							0.6678	0.7886	0.7881	0.9273	0.8598	0.7005	0.8115	0.8105	0.9515	0.8743
DMSO																
a							−0.4599	−0.5161	−0.5142	−0.5532	−0.5563	−0.4833	−0.5359	−0.5344	−0.5959	−0.5714
b							18.911	20.362	20.316	21.317	21.397	19.214	20.546	20.508	22.059	21.437
R^2							0.5997	0.7284	0.7292	0.7961	0.8033	0.6272	0.7448	0.7451	0.8914	0.8048

The numbering of atoms refers to Fig. 1.
* Calculation performed at B3LYP/6-31G* level.
** Calculation performed at B3LYP/6-311G** level.

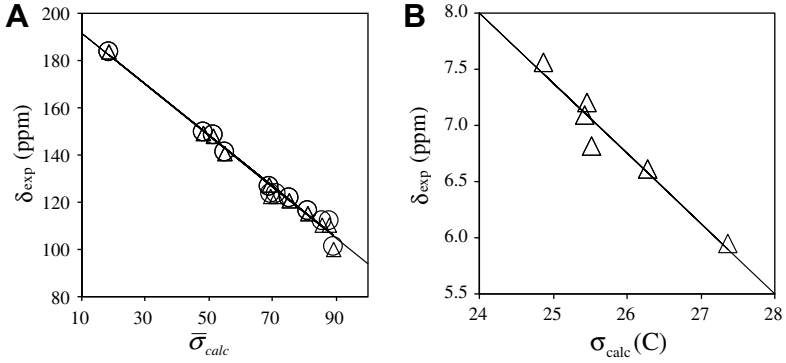

Fig. 6. Experimental chemical shifts of Curcumin vs. isotropic magnetic tensors from GIAO/B3LYP/6-311G** calculations for ^{13}C (A) and ^{1}H (B) in DMSO (○) and MeOD (Δ).

Table 5
Absorption wavelengths (λ) and oscillator strengths (f) for all Curcumin keto-enolic forms

		*	**	*	**	*	**	*	**	*	**
A	*E* (ev)	2.9626	2.9428	3.3314	3.305	3.4377	3.4627	3.646	3.6418	3.6957	3.6891
	λ (nm)	418.49	421.31	372.17	375.14	360.66	358.06	340.06	340.45	335.49	336.08
	f	1.5218	1.5164	0.0321	0.0316	0	0	0.1259	0.1366	0.0282	0.0288
BI	*E* (ev)	2.9749	2.9565	3.3603	3.3373	3.4344	3.4592	3.6173	3.606	3.6809	3.6691
	λ (nm)	416.77	419.36	368.97	371.51	361.01	358.42	342.76	343.83	336.83	337.92
	f	1.5198	1.5183	0.031	0.0311	0	0	0.1007	0.106	0.0082	0.0081
BII	*E* (ev)	2.9734	2.9555	3.3497	3.3257	3.4366	3.4618	3.6368	3.6309	3.6575	3.6911
	λ (nm)	416.97	419.5	370.13	372.8	360.77	358.15	340.92	341.47	338.99	335.9
	f	1.5181	1.5149	0.0399	0.0418	0	0	0.0841	0.0892	0.0301	0.0317
C	*E* (ev)	2.9882	2.9717	3.3809	3.3604	3.435	3.4606	3.609	3.6023	3.6657	3.6531
	λ (nm)	414.91	417.21	366.72	368.96	360.94	358.27	343.54	344.18	338.23	339.4
	f	1.5221	1.5259	0.0293	0.0283	0	0	0.0611	0.0621	0.0114	0.0119

* Stands for calculation performed at B3LYP/6-31G* level.
** Stands for calculation performed at B3LYP/6-311G** level.

which are determined on the basis of the relative species populations according to the following equation:

$$\bar{\nu}_{calc} = \bar{\nu}_{calc}(A)\cdot n_A + \bar{\nu}_{calc}(BI)\cdot n_{BI} + \bar{\nu}_{calc}(BII)\cdot n_{BII} + \bar{\nu}_{calc}(C)\cdot n_C$$

n_A, n_{BI}, n_{BII} and n_C are species populations determined by means of ΔG values with the exclusion of negligible di-keto form.

This result suggests that the over-estimation of calculated wavenumbers is quite systematic and allows to predict FT-IR spectra. Overlapping outcomes are obtained using the two different calculation levels B3LYP/6-31G* and B3LYP/6-311G**.

In conclusion, the comparison between experimental and theoretical data advises that calculated predictions are reliable even

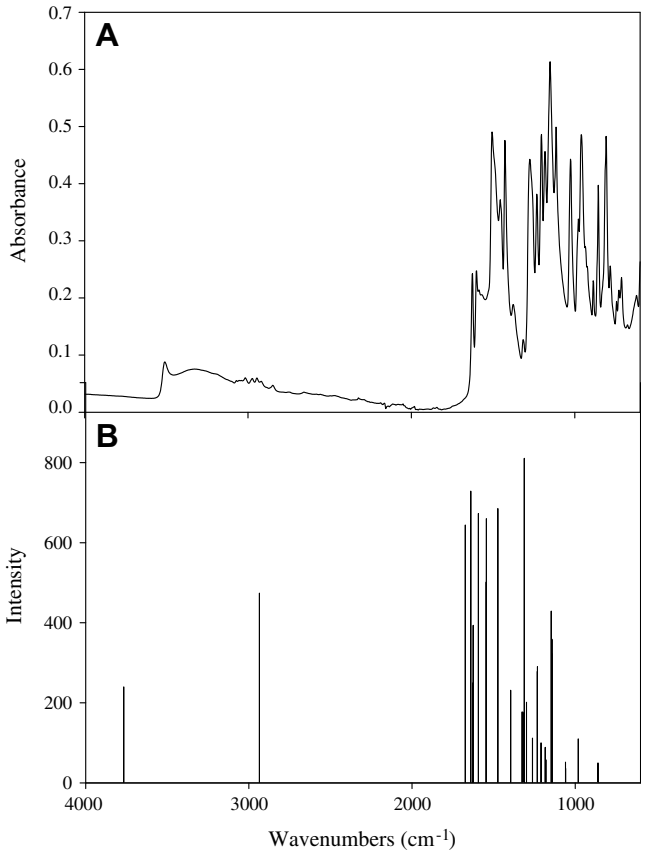

Fig. 7. Experimental spectrum of Curcumin: (A) FT-IR spectrum. (B) Calculated spectrum at B3LYP/6-311G** level of theory. Calculated wavelengths and intensity are estimated as averaged values on the basis of relative populations of keto-enolic species.

Table 6
More relevant IR vibration frequencies (cm^{-1}) and relative intensity – experimental and calculated ($\bar{\nu}_{calc}$) with B3LYP/6-311G** basis set

Calculated		Experimental	
$\bar{\nu}_{calc}$ (cm^{-1})	Intensity (km/mol)	ν (cm^{-1})	*A*
860.49	50.030	808.04	0.483
981.90	110.354	960.39	0.486
1059.40	52.151	1025.96	0.443
1147.33	429.491	1112.74	0.496
1179.93	58.140	1135.88	0.450
1209.45	100.366	1151.31	0.613
1231.68	290.468	1182.17	0.456
1262.26	112.022	1203.38	0.486
1312.32	811.020	1232.71	0.381
1325.99	177.591	1274.74	0.443
1474.56	685.852	1427.09	0.476
1544.87	660.324	1506.16	0.490
1625.33	393.85	1587.15	0.214
1639.75	729.055	1600.65	0.247
1673.97	644.472	1625.73	0.243
2935.38	474.413	2846.46	0.047
3766.63	240.171	3507.94	0.088

using relatively small basis set, such as B3LYP/6-31G*, which can be satisfactory implied to predict spectroscopic properties for complex organic structures, reducing computational efforts.

Acknowledgments

We are thankful to the "Consorzio Interuniversitario per il Calcolo Automatico dell'Italia Nord Orientale – CINECA" and to the "Laboratorio di Calcolo Scientifico Avanzato Interdipartimentale dell'Università degli Studi di Modena e Reggio Emilia" for computing facilities.

We are grateful to the "Centro Interdipartimentale Grandi Strumenti – C.I.G.S." of the University of Modena and Reggio Emilia and to the "Fondazione Cassa di Risparmio di Modena" for supplying NMR spectrometer.

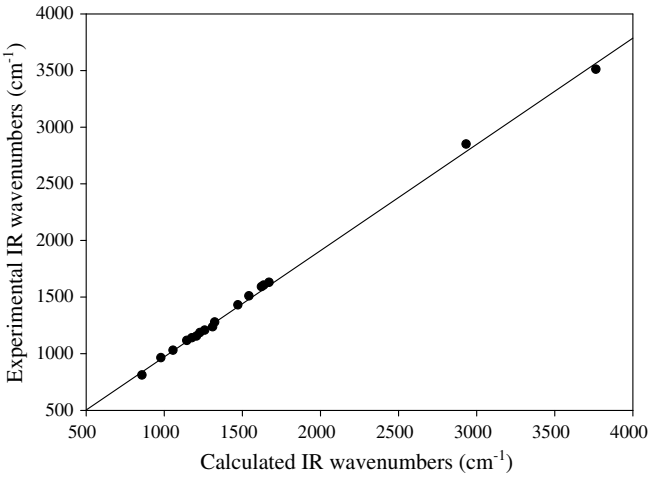

Fig. 8. Correlation between experimental and B3LYP/6-311G** *in vacuum* calculated wavenumbers for Curcumin. Equation: $\bar{\nu}_{exp} = a \cdot \bar{\nu}_{calc} + b$; $a = 0.9379$, $b = 34.449$, $R^2 = 0.9983$.

Appendix A. Supplementary data

Supplementary data associated with this article can be found, in the online version, at doi:10.1016/j.molstruc.2008.05.024.

References

[1] R.A. Sharma, A.J. Gescher, W.P. Steward, Eur. J. Cancer 41 (2005) 1955.
[2] B.B. Aggarwal, S. Shishodia, Biochem. Pharmacol. 71 (2006) 397.
[3] R.K. Maheshwari, A.K. Singh, J. Gaddipati, R.C. Srimal, Life Sci. 78 (2006) 2081.
[4] S. Gafner, S.K. Lee, M. Cuendet, S. Barthelemy, L. Vergnes, S. Labidalle, R.G. Mehta, C.W. Boone, J.M. Pezzuto, Phytochemistry 65 (2004) 2849.
[5] B.K. Adams, J. Cai, J. Armstrong, M. Herold, Y.J. Lu, A. Sun, J.P. Snyder, D.C. Liotta, D.P. Jones, M. Shoji, Anticancer Drugs 16 (2005) 263.
[6] B.B. Aggarwal, A. Kumar, A.C. Bharti, Anticancer Res. 23 (2003) 363.
[7] M.M. LoTempio, M.S. Veena, H.L. Steele, B. Ramamurthy, T.S. Ramalingam, A.N. Cohen, R. Chakrabarti, E.S. Srivatsan, M.B. Wang, Clin. Cancer Res. 11 (2005) 6994.
[8] S. Jovanovic, S. Steenken, C. Boone, M. Simic, J. Am. Chem. Soc. 121 (1999) 9677.
[9] K. Balasubramanian, J. Agric. Food Chem. 54 (2006) 3512.
[10] M. Borsari, E. Ferrari, R. Grandi, M. Saladini, Inorg. Chim. Acta 328 (2002) 61.
[11] M.J. Frisch, G.W. Trucks, H.B. Schlegel, G.E. Scuseria, M.A. Robb, J.R. Cheeseman, V.G. Zakrzewski, J.A.jr Montgomery, R.E. Stratmann, J.C. Burant, S. Dapprich, J.M. Illam, A.D. Daniels, K.N. Kudin, M.C. Strain, O. Farkas, J. Tomasi, V. Barone, M. Cossi, R. Cammi, B. Mennucci, C. Pomelli, C. Adamo, S. Clifford, J. Ochterski, G.A. Petersson, P.Y. Ayala, Q. Cui, K. Morokuma, D.K. Malick, A.D. Rabuck, K. Raghavachari, J.B. Foresman, J. Cioslowski, J.V. Ortiz, B.B. Stefanov, G. Liu, A. Liashenko, P. Piskorz, I. Komaromi, R. Gomperts, R.L. Martin, D.J. Fox, T. Keith, M.A. Al-Laham, C.Y. Peng, A. Nanayakkara, C. Gonzalez, M. Challacombe, P.M.W. Gill, B.G. Johnson, W. Chen, M.W. Wong, J.L. Andres, M. Head-Gordon, E.S. Replogle, J.A. Pople, Gaussian 03; Gaussian, Inc.: Pittsburgh, PA, USA, 2003.
[12] A.D. Becke, Phys. Rev. A 38 (1988) 3098.
[13] C. Lee, W. Yang, R.G. Parr, Phys. Rev. B 37 (1988) 785.
[14] R.E. Stratmann, G.E. Scuseria, M.J. Frish, J. Chem. Phys. 109 (1998) 8218.
[15] J.S. Murray, K.D. San (Eds.), Molecular Electrostatic Potentials: Concepts and Applications; Theoretical and Computational Chemistry Book Series, vol. 3, Elsevier, Amsterdam, 1996.
[16] R. Dennington II, T. Keyth, J. Millam, K. Eppinnett, W.L. Hovell, R. Gilliand, GaussView, Version 3.0, Semichem. Inc., Shawnee Mission, KS, 2003.
[17] S. Miertus, E. Scrocco, J. Tomasi, Chem. Phys. 55 (1981) 117.
[18] S. Miertus, J. Tomasi, Chem. Phys. 65 (1982) 239.
[19] M. Cossi, V. Barone, J. Cammi, Chem. Phys. Lett. 255 (1996) 327.
[20] K. Wolinski, J.F. Hinton, P.J. Pulay, J. Am. Chem. Soc. 112 (1990) 8251.

[21] K. Nagayama, A. Kumar, K. Wuethrich, R.R. Ernst, J. Magn. Res. 40 (1980) 321.
[22] A. Bax, M.F. Summers, J. Am. Chem. Soc. 108 (1986) 2093.
[23] A. Bax, R.H. Griffey, B.L. Hawkins, J. Magn. Res. 55 (1983) 301.
[24] H.H. Tonnesen, J. Karlsen, Acta Chem. Scand. B 36 (1982) 475.
[25] S.P. Paramiti, Y.V. Ramshanker, S. Suresh, T.N. Guru Row, Acta Cryst. E63 (2007) o860–o862.
[26] Y. M Sun, R.X. Wang, S.L. Yuan, X.J. Lin, C.B. Liu, Chin. J. Chem. 22 (2004) 827.
[27] K. Ling, K.I. Priyadarsini, H.Y. Zhang, J. Mol. Struct. (THEOCHEM) 684 (2002) 111.
[28] L. Shen, H.F. Ji, H. Y Zhang, Chem. Phys. Lett. 409 (2005) 300.
[29] L. Shen, H.F. Ji, Spectrochim. Acta A 67 (2007) 619.
[30] C. Ghio, G. Alagona, Int. J. Quant. Chem. 108 (2008) 1840.
[31] M. Szafran, E. Bartoszak-Adamska, J. Koput, Z. Dega-Szafran, J. Mol. Struct. 844–845 (2007) 140.
[32] A.A. Gorman, V.S. Hamblett, V.S. Srinivasan, P.D. Wood, Phochem. Photobiol. 59 (1994) 389.
[33] K.I. Priyadarsini, D.K. Marty, G.H. Naik, M.S. Kumar, M.K. Unnikrishnan, J.G. Satav, H. Mohan, Free Radic. Biol. Med. 35 (2003) 475.
[34] M. Szafran, A. Katrusiak, J. Koput, Z. Dega- Szafran, J. Mol. Struct. 846 (2007) 140.